Analysis and Visualization for Multiscale Control of Geologic CO2

Daniela M . Ushizima[1], Gunther H. Weber[1], Jonathan Ajo - Franklin[2], Yongman Kim[2], Alastair Macdowell[3], Dmitriy Morozov[1], Peter Nico[2], Dula Parkinson[3], David Trebotich[1], Jiamin Wan[2], Wes Bethel[1]

[1]Computational Research Division, Lawrence Berkeley National Laboratory,CA
[2]Earth Science Division, Lawrence Berkeley National Laboratory, CA
[3]Advance Light Source Division, Lawrence Berkeley National Laboratory, CA

Email: dushizima@lbl.gov

Abstract: Many of the challenges at the Energy Frontier Research Center are associated with understanding the processes in fluid-rock systems for geologic sequestration of CO_2, and developing technology for the safe storage of CO_2 in deep subsurface rock formations. This paper describes ongoing research in analysis of experimental data, including videos of CO_2 capillary trapping and dissolution, and computerized tomograms of porous materials. We discuss how we tackle visualization of numerical simulation output in key target areas as computing reaction rate in terms of the permeability based on inlet and outlet conditions of the porous media.

1. Introduction

The objective of the Energy Frontier Research Center (EFRC) for Nanoscale Control of Geologic CO_2 (NCGC) is to investigate the processes that play a role in geologic sequestration of CO_2 in fluid-rock systems. Such understanding is required to develop the technology needed for safely storing CO_2 in deep subsurface rock formations. Geologic sequestration of CO_2 is being pursued as a means of reducing the amount of CO_2, one of the principal greenhouse gases, being released into the atmosphere by processes that burn fossil fuels.

The NCGC investigates processes in fluid-rock systems from the molecular scale to the pore scale. They generate large amounts of experimental data for different parameters, e.g. variation of brine mixtures at different temperature and pressure values in porous media, while keep tracking of immiscible fluid structures, dissolution, and precipitation [11]. Numerical computer models calculate fluid-rock mechanics at pore scales, infiltration stability and instabilities, and emergent structures. Understanding these processes is key to describe flow and reactive transport of CO_2-rich fluids in geologic reservoirs and to develop approaches for controlling the flow of CO_2 in reservoirs that effectively and efficiently fill pore space with injected CO_2. Another member of the EFRC that we collaborate with is the Advance Light Source (ALS), particularly its Beamline 8.3.2, which permits tomographic monitoring of fluid invasions of 3D porous materials, precipitation, and dissolution [1].

Our work in collaboration with EFRC includes analysis and visualization of both experimental data and numerical simulation outputs in some key target areas. We have built image processing capabilities that can extract fluid and material quantities from experimental data to measure key phenomena, so we can later initialize, calibrate, and check numerical simulations. Our algorithms allow detection of carbon dioxide in porous materials, quantification of CO_2 during flow, and recovery of material structures from micro-CT. We visualize and analyze time-dependent behavior of numerical simulations by displaying simulation results along with derived diagnostic quantities like reaction rate.

This paper describes three different modules, with peculiar material, methods and results. Therefore, we dedicate a self-contained separate section for each of these modules. Section 2 describes the source data and algorithms used for quantitative image analysis in order to automate measurements

from videos of CO_2 dissolution at the pore scale (micrometer), including results of the 2D image analysis evolving in time. In order to deal with image analysis at a larger scale (μm to cm), and in 3D, Section 3 introduces a pipeline for extracting porosity parameters from micro computerized tomograms of porous samples, imaged at the ALS. Finally, Section 4 describes techniques to visualize reaction rates in simulation data, with discussions in Section 5.

2. CO_2 transport and flow on video

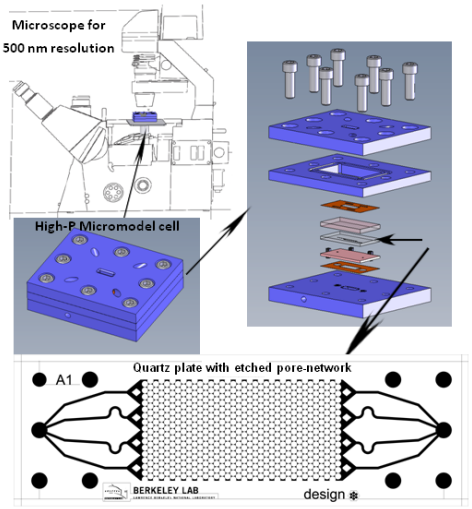

Figure 1. Experimental setup uses a transparent and homogeneous porous network for imaging the multiphase flow, phase displacement, wettability alteration, and sc-CO_2 residual trapping as a model to study CO_2 transport quantitatively. Courtesy: Jiamin Wan's laboratory, LBNL.

To quantify the spatial distribution of CO_2, an experimental setup was designed as illustrated in Fig. 1. Here, the porous medium consists of a quartz plate with an etched pore network, composed of 560 grains, of 580 μm diameter, subjected to varying values of pressure and temperature. Wan's laboratory [10] experimental setup has control of high-P interfacial tension and contact angle measurements, so that it is possible to image and measure supercritical CO_2-brine interfacial tensions under pressure up to 300 bar, temperature up to 100^oC and under controlled brine chemistry conditions. One new tool is a high-P/T transparent 2D porous medium, which allows imaging of multiphase flow, phase displacement, wettability alteration, and super-critical (sc) CO_2residual trapping.

We focus on the analysis of videos of the homogeneous porous network for quantitative transport studies. We designed an algorithm that detects the spatial distribution of super critical (sc) CO_2at pore and pore network scales during the post-injection stage, under conditions relevant to deep reservoir CO_2 sequestration. Our algorithm for coverage area vs. time of micromodel (CATM) measurement has 3 main stages:

The first stage consists of segmenting the template by processing a picture of the porous network before the injection of fluids and at the same focal distance the video will be recorded. From the template, we observed that it is possible to select a single and small patch (a.k.a. control-matrix template) and determine parameters necessary to align the video frames to a common coordinate system. These parameters enable rotation and translation of any video frame with respect to the template image (pore network only).

Since the image acquisition device is subjected to displacements, the second stage must include a registration procedure [7] and takes into account the parameters calculated in the stage 1. Here, a particular video frame is rotated and translated automatically before the calculation of its spatial correlation with the control-matrix. The maximum of the spatial correlation [5] result determines the exact position for the alignment of that particular frame with the template.

At the third stage, the algorithm eliminates the pore area and keep the area that can be invaded by brine and/or CO_2, which is followed by searching for "bubbles" of carbon dioxide in that area. Next, we enhance the contrast of the image by running the contrast-limited adaptive histogram equalization algorithm [12], modeling the histogram with an uniform distribution. Then, we "homogenize the detected liquids" by performing a binarization, considering only gray levels smaller than a threshold, determined empirically, here equal to 160, followed by the application of morphological operators to fill holes. The result is the coverage area corresponding to sc-CO_2.

2.1 Result: dissolution rate of residual CO_2

We analysed 5,578 images of 2848 x 4288 pixels, composing a video of approximately 417 minutes. Fig.2 shows the output for each step of the CATM algorithm, with template determination of the micromodel alone (before injecting brine and CO_2) for later registration. Then, for each frame, we

use a subimage (Fig.2.a) of the micromodel to be correlated to the control-matrix. After finding the best alignment to the pore network, as in Fig.2.c, the algorithm removes the pore network before segmentation of the remaining area into CO_2 and substrate-brine area. Next, we calculate the coverage area vs. time for the whole video, as illustrated in Fig.3, where the x-axis indicates time in seconds and y-axis is dissolution, calculated as the ratio B/A, where B is the area that was actually invaded by CO2 and A is the micromodel area that can be invaded by fluids. Each point represents an analyzed image, although the graph illustrates only points that are 30 seconds apart while the acquisition is at every 3 seconds.

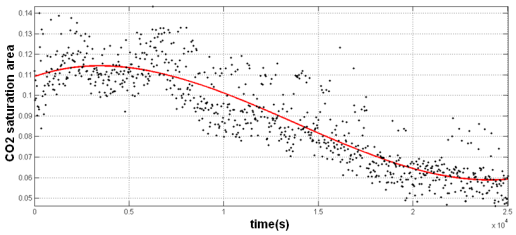

Figure 3. Percentage of sc-CO_2 saturation area during 417 minutes monitoring of a filling evacuated micromodel with 85 bar CO_2 saturated at 1M NaCl at 50^0C for dissolution study.

Our algorithm quantifies the dissolution rate of the residual CO_2 by means of calculating the ratio between the detected sc-CO_2 and the area that can be invaded by fluids. The graph in Fig. 3 shows the dispersion for the area percentage values, mostly due to artifacts during the remotion of the pore by using the template. In spite of the accuracy limitations, it enabled the analysis of the experiments for several minutes and correctly detected that the concentration of sc-CO_2 decays along the experiment.

This section described research using homogeneous porous network under conditions relevant to understand geochemical reactions and transport in multiphase subsurface systems, particularly those involving interfacial phenomena. The next section addresses algorithms to describe the substrate, where transport may take place, based on the porosity properties of the material.

3. Analysis of porous material from synchrotron micro-tomography images

Porous materials imaged using synchrotron-based X-ray spectromicroscopy (beamline 8.3.2 at the Advanced Light Source [2]) are represented as a 3D stack of 2D slices. We use this source of data as input to nondestructive techniques that quantify properties in the interior of solid objects, including information about their 3D geometries. This quantification may support modeling of the fluid dynamics into the pore space of the host object. Our pipeline filters, segments and extracts features from porous media with potential applications to carbon sequestration research.

One of the challenges is to minimize the image artifacts (fringes), which generate false sharp borders. Our framework controls spurious heterogeneity of the image using 2D bilateral filtering [9], an edge preserving smoothing technique that allows tuning of a stencil for eliminating false contrasts. Next, a segmentation algorithm splits blocks of the volume into homogeneous regions, calculating the pertinence of a certain pixel/region to be part of a larger region. This merging requires a statistical test

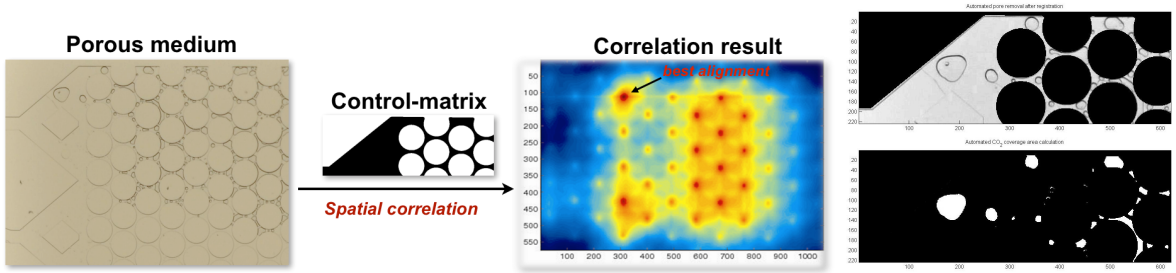

(a) (b) (c) (d)

Figure 2. CATM pipeline: image patch from the transparent porous medium (a) undergoes spatial correlation calculation using the control matrix (b), followed by detection of best alignment (c); (d) ilustrates the segmentation: partition of the image into sc-CO_2 area and subtrate-brine area.

to check if the mean intensities are similar enough for the regions to be merged, which is based on the deviation of observed differences between regions of the image [8].

To analyze the physical properties of the material, as well as compare the results from experiments and simulation, we summarize the geometry of the pores. By extracting an (annotated) graph that reflects their connectivity, we provide a compact descriptor that can be used to quantitatively characterize the material. We illustrate the application of such a pipeline to a Fe-sand porous material placed inside a metallic cylinder, with dimensions 1813 x 1813 x 510 pixels at 1.7 μm.

3.1 Result: porosity of micro-CT hyperstacks

Given a stack of image slices, our framework classifies the porous media into solid and empty spaces. Fig.4 illustrates it can be applied to high-resolution x-ray micro-tomography images. First, the user selects the region of interest from a slice (e.g. sample inside the cylinder), these parameters will be used for all other slices. Next, a border preserving filter minimizes fringes and streaks while augmenting the contrast between solid and empty spaces.

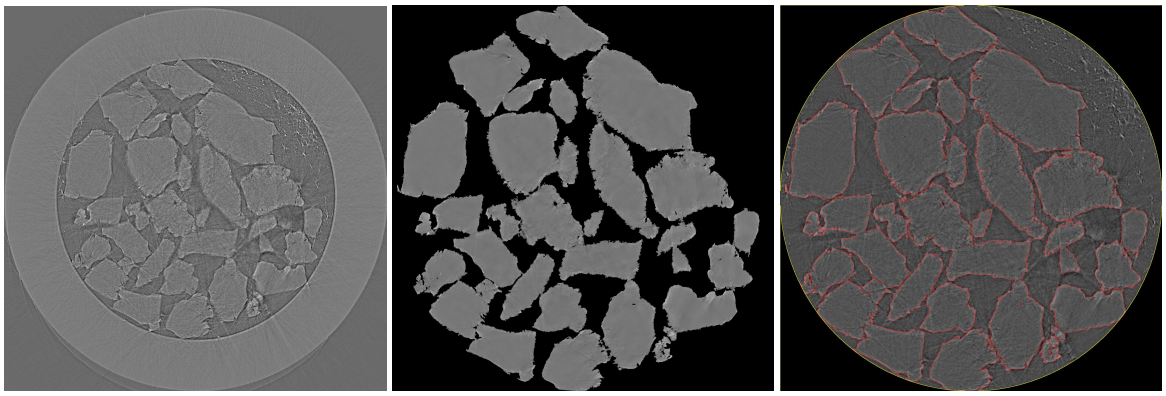

(a) (b) (c)

Figure 4. (a) Slice of porous material, after reconstruction from x-ray beams; (b) region of interest from sample in the cylinder, after range-domain filtering; (c) borders of segmentation result overlaid on image (a) .

Then, the algorithm performs classification of the pixels into regions, maintaining the average gray level for each region. The final step outputs a binary image by running a standard fuzzy thresholding algorithm, using Shannon's entropy function to determine the cut-off among the intensity values.

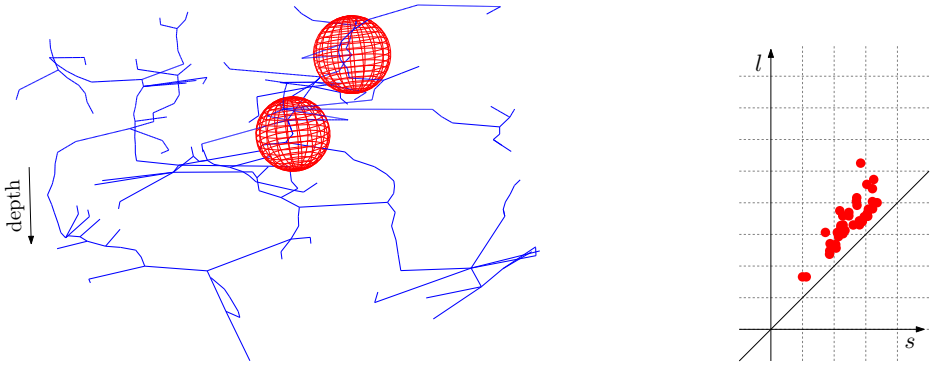

(a) (b)

Figure 5. (a) Reeb graph of the fat pores in the (down-sampled) data illustrated in Figure 4. Components shorter than the third of the height of the material are not shown. The two most persistent pockets are marked with the largest spheres that fit inside; (b) persistence diagram of the pockets of the same material with noisy (low-persistent) points removed.

The resulting binary classification lets us study the three-dimensional geometry of the pores. Our goal is both to visualize their internal structure and to be able to compare multiple materials. To this end, we extract a pair of multi-scalar geometric descriptors.

We restrict our view to the subspace of the pores where every point is the center of an empty sphere of a given radius r. At every depth d into the 3D stack of the images, we have a collection of connected components of this space. By collapsing each component, we get a Reeb graph [4]. This structure captures the topology of the "fat pores", i.e. of the empty space in the material that's thicker than the given threshold r. Figure 5(a) illustrates this construction for the solid volume, composed of slices as in Figure 4.

In addition to the graph of the fat pores, we use the theory of persistent homology [4, Chapter VII] to detect pockets within the material, where the liquid can accumulate. We say that a pocket has parameters (s,l) if the largest empty sphere that fits inside has radius l, while the largest sphere that can escape has radius s. The larger the difference $l - s$ between these radii, called persistence, the more significant is the pocket. By plotting all the pairs (s,l) in the plane, with s as the abscissa and l as the ordinate of the point, we get a persistence diagram, as shown in Figure 5(b); points further away from the diagonal represent more persistent pockets. The diagram serves as a guide to the material: it highlights significant scales, shows all the pockets at once, and allows the user to compare multiple materials.

4. Visualization of simulation data of flow in porous media

Members of the SciDAC Applied Partial Differential Equations Center (APDEC) are developing numerical modeling and simulation methods for the NCGC. This work centers around algorithm development for modeling two fluids—CO_2 and water—flowing and reacting in microscale pore space. The simulation methods employed are based on an embedded boundary/volume-of-fluid approach. Each cell of the computational grid has information specifying what fraction of the cell is filled with the various materials/fluids participating in the simulation. The simulation models the interface between individual materials as an implicit function and updates this function according to simulated chemical interactions.

Current simulations performed by APDEC consider only one phase (CO_2) and its flow around pores in the medium, which are modelled as packed spheres at different densities. Of primary interest is how these systems evolve over time. To visualize the temporal change of the system, we derive two quantities (i) the area normalized dissolution rate (i.e., reaction rate) [6] and permeability (i.e., resistance of the system) as a function of time. Approximations to both quantities are computed as sums of derived expressions (based species concentration, velocity and pressure) over a one cell wide slice at inlet and outlet, respectively. Using VisIt [3] with its ability to reconstruct material interfaces, to define derived quantities as expressions and to perform queries that compute sums over select regions of the simulation, we compute time curves of reaction rate and permeability. We then plot a curve that shows the evolution of these quantities. To correlate the behavior of this curve with behavior of the simulation, we display visualizations of the 2D or 3D simulation domain.

In Fig. 6, we display 2D pseudocolor plots of variables of interest (such as species concentrations or pressure). In these pseudocolor plots, values are mapped to colors, and each location is colored according to the function value at that location. For example, the left hand side of Fig. 6 shows the simulation of a sphere packing with 70% porosity. The pseudocolor plot shows the concentration of Ca^{2+} throughout the domain (with white disks signifying the positions of the packed sphere serving as an obstruction). The curve in the lower part shows how the reaction rate changes as a function of time. To correlate the current time step to the curve, a red line and dot highlight the current time step in the curve. When shown as animation, this setup serves well to illustrate the different stages along the curve. Initially the reaction rate slightly increases until the species hits the first packed spheres. Subsequently, there is a slow decrease as the concentration within the packed sphere region increases. The figure shows a time step at the end of the stage as the maximum species concentration is about to arrive at the outlet. As soon as this occurs, the reaction rate decreases very quickly. The right hand side of Fig. 6 shows a pseudocolor plot of pressure in the system, with curve below emphasizing how permeability of the system changes over time.

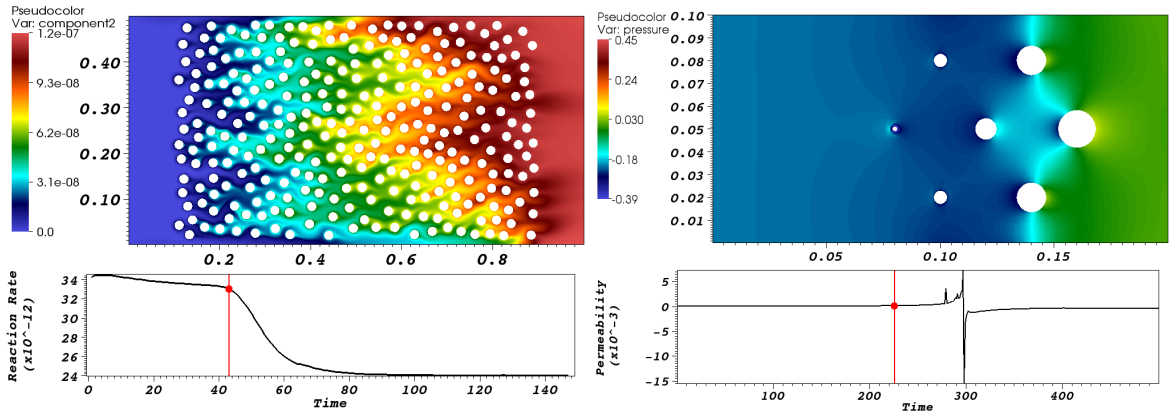

Figure 6. Visualizations correlating the temporal evolution of derived, per-timestep quantities (curve plot) to system state in the 2D physical simulation domain (pseudocolor plots): (Left)Concentration of Ca^{2+} (top) and reaction rate (bottom). (Right) Pressure (top) and permeability (bottom). The axes for the pseudocolor plots correspond to the spatial dimensions of the simulation domain.

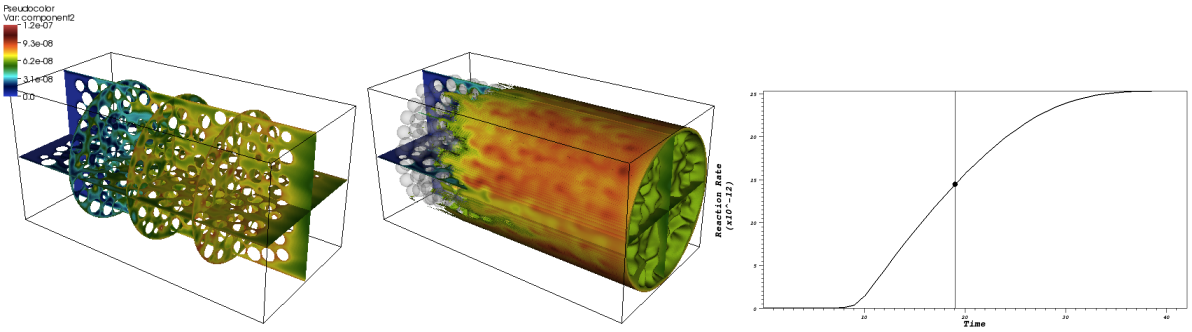

Figure 7. Visualization correlating temporal evolution of reaction rate (right) to 3D simulation views of flow through a packed cylinder (left, center). (Left) Pseudocolor plot of Ca^{2+} concentration on select axis-perpendicular slices (one slice for each axis through the simulation domain center and two additional x-perpendicular slices). (Center) Packed spheres rendered transparently to illustrate the 3D packing and volume corresponding to Ca^{2+} concentration above a threshold.

In 3D it is no longer possible to use a simple pseudocolor plot to show the variation of a variable withing the system. Instead we display quantities such as Ca^{2+} concentration on selected axes, perpendicular to slices (three slices perpendicular to the x-axis evenly through the simulation domain as well as one y-axis and one z-axis perpendicular slice through the simulation domain center), see the left panel of Fig. 7. In addition, we can show 3D visualizations of the system (middle panel of Fig. 7) for transparent packed spheres to simultaneously illustrate the packing and the volume corresponding to Ca^{2+} concentration above a certain threshold. As in the 2D case, we correlate this information with a curve plot (right panel) that shows the evolution of a derived quantity (reaction rate in the figure) as a function of time. A black dot and line mark the current visualized time step on this plot.

5. Conclusion/Discussion

Typical carbon dioxide sequestering layers include brine-soaked sandstone subsurface aquifers, therefore the analysis of micromodels is relevant since they resemble sandstone and allow investigation under brine-scCO_2 interaction. In a larger scale, we analyzed sandstone porous media and create methods to assess its permeability.

We developed quantitative image analysis methods to automate measurements of experimental data, proposed a framework to detect/reconstruct material interfaces for future quantification of CO_2

flow, to recover material structures from microCT and to visualize data from fluid flow simulations in porous material.

The calculation of sc-CO_2 dissolution in micro-models using videos of micro-model confirmed that trapped residual CO_2 is unstable - the algorithm should be improved to be more tolerant to pore shadows and/or the camera to be fixed during image acquisition.

We partitioned material with different density for structure reconstruction, using micro-CT and described its pore structure using Reeb-graphs and persistence diagrams. Also, we developed visualization algorithms to tackle simulation of fluid flow on pore network.

This new capability is a big step forward to the EFRC, increasing their ability to have scientific insights about their experiments and respective parametrization, compare different materials in terms of their persistence diagram as well as accelating the analysis of large amounts of data.

Future developments enclose evaluation of measurements in experimental data given ground-truth data, including comparison among different segmentation pipelines, description of permeability of pore network using persistence diagrams.

6. Acknowledgements

We thank Donald J. DePaolo, Center Director of Nanoscale Control of Geologic CO_2, an Energy Frontier Research Center. This work was partially supported by the Director, Office of Science, Office and Advanced Scientific Computing Research, of the U.S. Department of Energy under Contract No. DE-AC02-05CH11231 through the Scientific Discovery through Advanced Computing (SciDAC) and Visualization and Analytics Center for Enabling Technologies (VACET). Also, it was supported in part by the Applied Mathematical Science subprogram of the Office of Energy Research, U.S. Department of Energy, under Contract Number DE-AC03-76SF00098.

References

[1] Ajo-Franklin, J. [2010]. Using synchrotron micro tomography for pore-scale monitoring of $caco_3$ precipitation and co_2 flow, Symposium of Nanoscale Control of Geologic CO_2 - Energy Frontier Research Center, Berkeley, CA.

[2] ALS [2011]. Advanced Light Source, `http://www-als.lbl.gov/`.

[3] Childs, H., Brugger, E. S., Bonnell, K. S., Meredith, J. S., Miller, M., Whitlock, B. J. and Max, N. [2005]. A contract-based system for large data visualization, IEEE Visualization 2005, pp. 190–198.

[4] Edelsbrunner, H. and Harer, J. L. [2010]. Computational topology: An introduction, AMS .

[5] Gonzalez, R. C. and Woods, R. E. [2006]. Digital Image Processing (3rd Edition), Prentice-Hall, Inc., Upper Saddle River, NJ, USA.

[6] Li, L., Steefel, C. I. and Yang, L. [2008]. Scale dependence of mineral dissolution rates within single pores and fractures, Geochimica et Cosmochimica Acta **72**(2): 360 – 377.

[7] Merchant, F. [2008]. 3d imaging, Microscope Image Processing pp. 329–389.

[8] Nock, R. and Nielsen, F. [2004]. Statistical region merging, IEEE Transactions on Pattern Analysis and Machine Intelligence **26**: 1452–1458.

[9] Tomasi, C. and Manduchi, R. [1998]. Bilateral filtering for gray and color images, Proceedings of the Sixth International Conference on Computer Vision, ICCV '98, IEEE Computer Society, Washington, DC, USA, pp. 839–.

[10] Wan, J., Kim, Y., Ushizima, D., Kneafsey, T. and Tokunaga, T. [2010]. Developing laboratory capabilities to study co_2 capillary trapping and dissolution relations, Symposium of Nanoscale Control of Geologic CO_2 - Energy Frontier Research Center, Berkeley, CA.

[11] Wu, Y., Hubbard, S., Williams, K. H. and Ajo-Franklin, J. [2010]. On the complex conductivity signatures of calcite precipitation, Journal of Geophysical Research **115**(null): G00G04+.

[12] Zuiderveld, K. [1994]. Contrast limited adaptive histograph equalization, Graphic Gems IV pp. 474–485.